JOURNAL OF PROPULSION AND POWER
Vol. 23, No. 2, March–April 2007

Conceptual Study of a Rocket-Ramjet Combined-Cycle Engine for an Aerospace Plane

Takeshi Kanda,* Kouichiro Tani,† and Kenji Kudo‡
Japan Aerospace Exploration Agency, Kakuda 981-1525, Miyagi, Japan

DOI: 10.2514/1.22899

Operating conditions of a rocket-ramjet combined-cycle engine for a single-stage-to-orbit aerospace plane were studied. The engine was composed of an ejector-jet mode, a ramjet mode, a scramjet mode, and a rocket mode. Characteristics of the engine operating conditions were studied analytically. The thrust augmentation effect of the ejector-jet mode was found to be small at low subsonic speed and to increase with an increase of the flight Mach number. Study of the effective impulse function clarified that higher specific impulse was preferable in supersonic flight, whereas greater thrust coefficient was preferable in hypersonic flight. The mentioned characteristics were examined by simulation of engine operating in an aerospace plane flight. Transportation of a mass into orbit was compared among several engines with different combinations of thrust and specific impulse. The mass which could be carried into orbit was larger with a ramjet mode of higher specific impulse and with a scramjet mode of greater thrust.

Nomenclature

A	=	cross section
Ca	=	mass ratio of stoichiometric fuel to air
C_D	=	drag coefficient
C_F	=	thrust coefficient
D	=	drag
F	=	thrust
Isp	=	specific impulse
M	=	Mach number
m	=	mass
$\dot{m}$	=	mass flow rate
P	=	pressure
R	=	gas constant
r	=	mass flow ratio of rocket exhaust to airflow
S	=	planform area
T	=	temperature
t	=	time
u	=	velocity
ΔQ	=	heat release by combustion
Δv	=	velocity increment
γ	=	ratio of specific heats
ϕ	=	equivalence ratio

Subscripts

a	=	air
av	=	average
c	=	combustion gas
e	=	effective
eng	=	engine
f	=	fuel
flt	=	flight condition
$H2$	=	hydrogen
p	=	propellant
r	=	rocket
t	=	total
0	=	initial
1	=	final

Presented at the 17th International Symposium on Airbreathing Engines, Munich, Germany, 4–9 September 2005; received 31 January 2006; revision received 13 July 2006; accepted for publication 27 July 2006.

*Manager, Combined Propulsion Research Group, 1 Koganesawa, Kimigaya; kanda.takeshi@jaxa.jp. Senior Member AIAA.

†Leader, Engine Systems Section, Combined Propulsion Research Group, 1 Koganesawa. Member AIAA.

‡Senior Researcher, Engine Systems Section, Combined Propulsion Research Group.

I. Introduction

SEVERAL kinds of engines for an aerospace plane are now under investigation. When several engines are mounted on a vehicle, it is termed a combination propulsion system. When an engine operates in several modes, it is termed a combined-cycle engine [1]. In the combination propulsion system, each engine is predicted to show a high performance, although the engines of such a system will be heavier. During operation of one engine, additional engines may add drag. They will also add deadweight when turned off. Although the combined-cycle engine shows lower performance in each operating mode, it will be lighter and will not induce additional drag.

Study of the combined-cycle engine has a long history, and several kinds of such engines have been proposed and studied [2–4]. A well-known combined-cycle engine is the rocket based combined-cycle engine (RBCC) [5,6]. The RBCC is composed of an ejector-jet mode, a ramjet mode, a scramjet mode, and a rocket mode.

At the Japan Aerospace Exploration Agency, a rocket-ramjet combined-cycle engine is presently being studied [7–12]. It is composed of an ejector-jet mode, namely, an airbreathing rocket mode, as well as ramjet, scramjet, and rocket modes. The engine operates in the ejector-jet mode from takeoff to about Mach 3, in the ramjet mode from Mach 3 to Mach 7, and in the scramjet mode from Mach 7 to 11. Because this engine has the rocket mode, it is suitable for use in a single-stage-to-orbit (SSTO) aerospace plane. There are many design parameters of the rocket-ramjet combined-cycle engine, e.g., the contraction ratio of the inlet, the nozzle expansion ratio of the rocket, the pressure of the rocket chamber, and the mixture ratio of the rocket. Optimization of each parameter has relation to transition condition of each operating mode.

In the present study, engine operating conditions were examined analytically to clarify engine characteristics and to maximize transportation capacity of the engine. The results of the analysis were confirmed by numerical simulation of the operation of the engine in SSTO flying condition. In the calculation of the engine performance, a decelerating process in the ejector-jet mode and ramjet mode was improved by using a momentum balance model [13].

II. Combined-Cycle Engine and its Operating Conditions

Figure 1 shows the configuration of the SSTO aerospace plane with the combined-cycle engine. Figure 2 shows a schematic of the operating conditions of this engine. Propellants are liquid hydrogen and liquid oxygen for all modes. Figure 3 indicates the components of this engine and their dimensions.

Under the ejector-jet mode, namely, the airbreathing rocket mode, air is breathed in by the ejector effect of the rocket. Thrust is produced not only by the rocket engine itself, but also by the divergent section with the increased pressure of a mixture of air and rocket exhaust. Further subsonic combustion is attained by fuel injection from a second fuel injector [14]. In the ramjet mode, the rocket exhaust decreases to increase the specific impulse, and pressure recovery of the air is attained in the divergent section. In the scramjet mode, the ejector rockets work as a preburner to supply hot, fuel-rich gas.

A propellant feed system with umbilical ducts from the cryogenic propellant tanks will be mounted in the ejector rocket section. This is the heaviest section of the engine and will be difficult to move. In the model, this section and the following combustor section are fixed. There is no second throat at the exit of the engine. Subsonic combustion in the absence of a second throat configuration with choking was attained in the experiments of the ramjet mode operation [11,15]. With no second throat, the engine can be simplified and will be lighter. The contraction of the inlet is also fixed during operation. The inlet has a ramp-compression system. The ramp is movable and closes the inlet in the entry flight from an orbit [16].

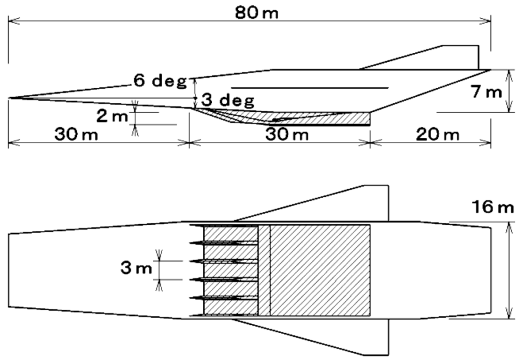

Fig. 1 Schematic of SSTO plane with combined-cycle engine.

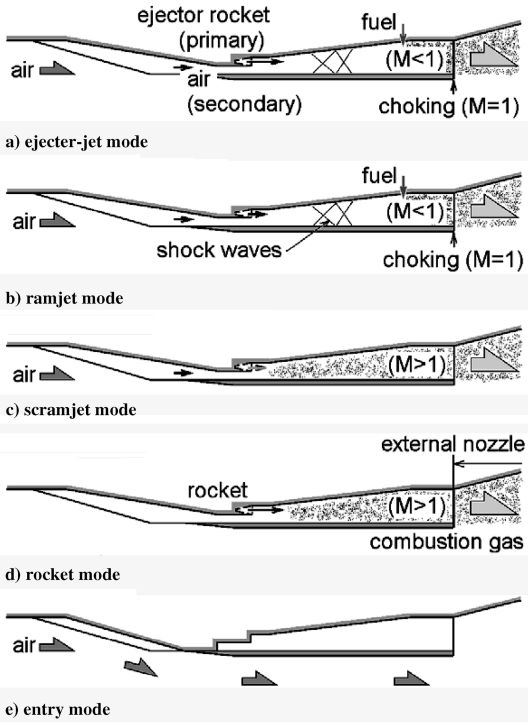

Fig. 2 Schematic of operating conditions of combined-cycle engine.

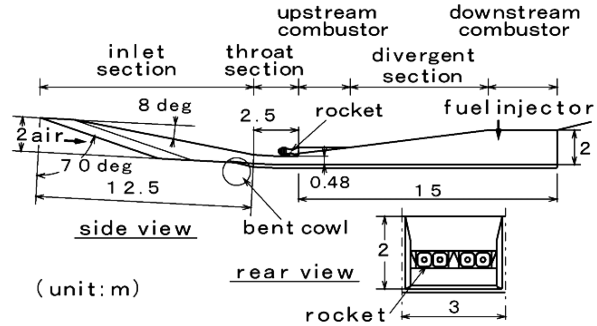

Fig. 3 Components and dimensions of combined-cycle engine.

III. Analytical Study on Operating Conditions

There have not been clear criteria for operating conditions of the ejector-jet, ramjet and, scramjet modes. Herein, the effect of breathing on thrust augmentation in the ejector-jet mode is examined analytically with simple equations. In the ramjet and scramjet modes, higher specific impulse does not always produce greater payload. Suitable operating conditions of the rocket were examined in the ramjet and the scramjet modes.

A. Ejector-Jet Mode

Thrust augmentation in the ejector-jet mode was examined. Energy conservation is expressed as follows:

$$(\dot{m}_a + \dot{m}_r)\left(\frac{1}{2}u_c^2 + h_c\right) \approx \dot{m}_a\left(\frac{1}{2}u_a^2 + h_a + \Delta Q_a\right) + \dot{m}_r \cdot \Delta Q_r \tag{1}$$

ΔQ_a is heat release at unit airflow rate due to combustion of air and fuel, whereas ΔQ_r is heat release due to combustion in rockets at the unit mass flow rate of rocket combustion gas. The fuel flow rate is much smaller than that of airflow, and so it is neglected here. An equivalence ratio is presumed to be unity.

Enthalpy is expressed with kinetic energy as follows:

$$h = \frac{1}{2}u^2 \cdot \frac{2}{(\gamma - 1)M^2} \tag{2}$$

When combustion gas chokes at the exit of the engine, velocity at the exit is expressed by Eqs. (1) and (2) as follows:

$$u_c = \sqrt{\frac{2(\gamma_c - 1)}{\gamma_c + 1}\frac{\left\{\dot{m}_a\left[(1/2)u_a^2 + h_a + \Delta Q_a\right] + \dot{m}_r \cdot \Delta Q_r\right\}}{\dot{m}_a + \dot{m}_r}} \tag{3}$$

Thrust of the engine is expressed as follows:

$$F_{\text{eng}} = (\dot{m}_a + \dot{m}_r) \cdot u_c + P_c \cdot A_c - (\dot{m}_a \cdot u_a + P_a + A_a) \tag{4}$$

Mass flow rate is expressed as follows:

$$\dot{m} = PA \cdot M\sqrt{\frac{\gamma}{RT}} \tag{5}$$

Then

$$PA = \frac{\dot{m}}{M}\sqrt{\frac{R \cdot T_t}{\gamma}}\frac{1}{\sqrt{1 + [(\gamma - 1)/2]M^2}} \tag{6}$$

Here

$$h_{tc} = \frac{\gamma_c}{\gamma_c - 1} R_c \cdot T_{tc} = \frac{\dot{m}_a[(1/2)u_a^2 + h_a + \Delta Q_a] + \dot{m}_r \cdot \Delta Q_r}{\dot{m}_a + \dot{m}_r} \tag{7}$$

With Eq. (7), the pressure term of Eq. (4) is expressed as follows in the choking condition

$$P_c A_c = (\dot{m}_a + \dot{m}_r)\sqrt{\frac{2(\gamma_c - 1)}{\gamma_c^2(\gamma_c + 1)} \frac{\dot{m}_a(h_{ta} + \Delta Q_a) + \dot{m}_r \Delta Q_r}{\dot{m}_a + \dot{m}_r}} \tag{8}$$

With Eqs. (3), (7), and (8), Eq. (4) is expressed as follows:

$$F_{\text{eng}} = (\dot{m}_a + \dot{m}_r)\left(\sqrt{\frac{2(\gamma_c - 1)}{\gamma_c + 1} \frac{\dot{m}_a(h_{ta} + \Delta Q_a) + \dot{m}_r \Delta Q_r}{\dot{m}_a + \dot{m}_r}} + \sqrt{\frac{2(\gamma_c - 1)}{\gamma_c^2(\gamma_c + 1)} \frac{\dot{m}_a(h_{ta} + \Delta Q_a) + \dot{m}_r \Delta Q_r}{\dot{m}_a + \dot{m}_r}}\right) - (\dot{m}_a u_a + P_a A_a) \tag{9}$$

Or

$$F_{\text{eng}} = \sqrt{\frac{2(\gamma_c - 1)}{\gamma_c + 1}}\left(1 + \frac{1}{\gamma_c}\right) \times \sqrt{(\dot{m}_a + \dot{m}_r)\left[\dot{m}_a\left(\frac{\gamma_a}{\gamma_a - 1} R_a T_{ta} + \Delta Q_a\right) + \dot{m}_r \Delta Q_r\right]} - \dot{m}_a \sqrt{\frac{\gamma_a R_a T_{ta}}{1 + [(\gamma_a - 1)/2]M_a^2}}\left(M_a + \frac{1}{\gamma_a M_a}\right) \tag{10}$$

At the exit of the rocket nozzle, kinetic energy is larger than static enthalpy of the combustion gas. In the rocket combustion chamber, heat release by combustion is larger than enthalpy before combustion. Then, energy conservation of the rocket is as follows:

$$\frac{1}{2}u_r^2 + h_r = h_p + \Delta Q_r \qquad \frac{1}{2}u_r^2 \approx \Delta Q_r \tag{11}$$

$$u_r \approx \sqrt{2\Delta Q_r} \tag{12}$$

Then

$$F_r = \dot{m}_r \cdot u_r + P_r \cdot A_r \approx \dot{m}_r \sqrt{2\Delta Q_r} \tag{13}$$

This is ideal thrust of a rocket in a vacuum condition. The thrust of a rocket in a flight condition is as follows:

$$F_{ra} = F_r - A_r \cdot P_{ta} \tag{14}$$

Figure 4 shows F_{eng}/F_{ra} when inflow air is choked at the throat. Outflow and inflow impulse functions are normalized with the thrust of the rocket calculated by Eq. (14). Static pressure of the inflow air was 100 kPa. As the flight Mach number increased, flight-dynamic pressure increased. Here, propellants were hydrogen and oxygen. $\Delta Q_a = 3.53\ \text{MJ} \cdot \text{kg}^{-1}$, $\Delta Q_r = 13.4\ \text{MJ} \cdot \text{kg}^{-1}$, $(\text{O/F})_r = 8$ of the rocket, $R_a = 289\ \text{J} \cdot \text{kg}^{-1} \cdot \text{K}^{-1}$, the reference chamber pressure of the rocket is $P_c = 5$ MPa, the cross section at the engine entrance is $A_a = 30\ \text{m}^2$, the reference contraction ratio of the inlet is CR = 3.5, the throat section of the rocket is $A_{\text{tr}} = 0.3\ \text{m}^2$, and ratios of specific heats are $\gamma_c = 1.3$, $\gamma_r = 1.2$, and $\gamma_a = 1.4$.

The augmentation of thrust against the rocket thrust was approximately constant in a subsonic condition. Though the outflow impulse function in Eq. (9) increased, the inflow impulse function, which is indicated in negative value, also increased with flight Mach number. Therefore, F_{eng}/F_{ra} was almost constant in subsonic flight.

It should be noted that the engine thrust calculated with Eq. (9) has no relation to the engine duct configuration. That is, there is no assurance that the impulse function at the exit can be produced in the engine. As the inlet contraction ratio decreases, the divergent section downstream of the rockets decreases, that is, thrust production area in the engine decreases. In a small contraction condition, therefore, thrust cannot be augmented in the engine. At the same time, breathing of air and its choking become difficult in a condition of a small flow rate of the rocket exhaust relative to the airflow rate [17].

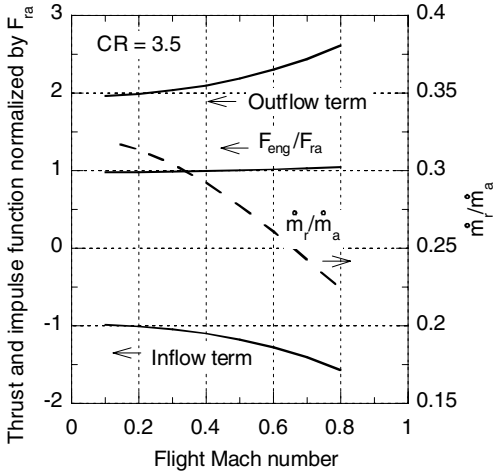

Fig. 4 Thrust augmentation and ratio of mass flow rates against flight Mach number.

B. Ramjet Mode

Potential energy of an aerospace plane at a low-earth orbit is sufficiently smaller than kinetic energy of the vehicle. The velocity increment is expressed with drag and thrust as follows:

$$\Delta v = Isp \cdot \left(1 - \frac{D}{F_{\text{eng}}}\right) \ell_n \frac{m_0}{m_1} = Isp \cdot \left(1 - \frac{S \cdot C_D}{A_a \cdot C_F}\right) \ell_n \frac{m_0}{m_1} = Isp_e \cdot \ell_n \frac{m_0}{m_1} \tag{15}$$

In this section, the effective specific impulse, $Isp_e = Isp \cdot (1 - D/F_{\text{eng}})$, is examined.

In the ramjet mode, combustion gas is choked at the exit of the engine. Equation (9) is also used for the engine thrust in the ramjet mode. Airflow is not choked at the throat and the contraction ratio of the inlet is not a parameter here. In the ramjet mode, the flow rate of the rocket exhaust is small, whereas the fuel flow rate is large. The fuel flow rate is expressed explicitly in the denominator of the equation of specific impulse.

Specific impulse is expressed as follows:

$$Isp = \frac{F_{\text{eng}}}{\dot{m}_r + \dot{m}_f} = \sqrt{\frac{2(\gamma_c - 1)}{\gamma_c + 1}} \cdot \left(1 + \frac{1}{\gamma_c}\right) \frac{\dot{m}_a + \dot{m}_r}{\dot{m}_r + Ca \cdot \dot{m}_a} \times \sqrt{\frac{\dot{m}_a(h_{ta} + \Delta Q_a) + \dot{m}_r \Delta Q_r}{\dot{m}_a + \dot{m}_r}} - \frac{\dot{m}_a u_a + P_a A_a}{\dot{m}_r + Ca \cdot \dot{m}_a} \tag{16}$$

Here

$$\dot{m}_f = Ca \cdot \dot{m}_a \tag{17}$$

Fuel flow rate is estimated with a mass ratio of stoichiometric hydrogen fuel to air of 1/34.3. Thrust and drag are expressed as follows:

$$F_{\text{eng}} \approx C_F \cdot \frac{1}{2}\dot{m}_a \cdot u_a \tag{18}$$

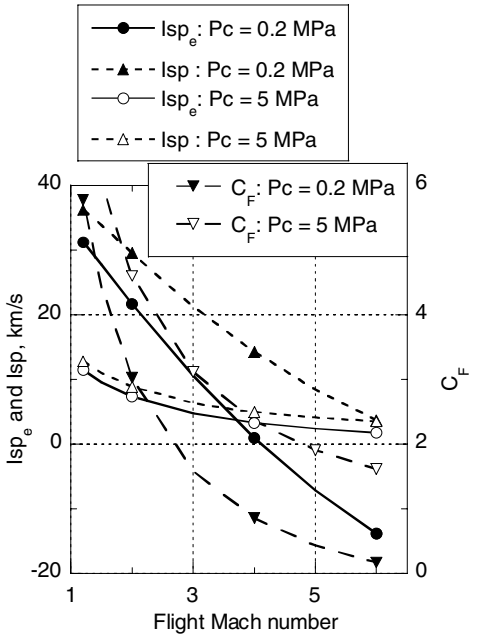

Fig. 5 Isp_e, Isp, and C_F against flight Mach number. Rocket chamber pressure P_c is a parameter.

$$D \approx C_D \cdot S \cdot \frac{\dot{m}_a \cdot u_a}{2A_a} \tag{19}$$

The precompression effect on airflow into the engine by the forebody of the airframe and the three-dimensional effect are neglected for simplification. The choking condition of the combustion gas at the engine exit is the same as that of the ejector-jet mode. Thus, the ratio of thrust to drag is expressed with Eqs. (10) and (19) as follows:

$$\frac{F_{\text{eng}}}{D} = \frac{F_{\text{eng}} \times 2A_a}{C_D \cdot S \cdot \dot{m}_a \cdot u_a} = \frac{2A_a}{C_D \cdot S}\left[\frac{1}{M_a}\sqrt{1+\frac{\gamma_a-1}{2}M_a^2}\left(1+\frac{1}{\gamma_c}\right)\right.$$
$$\times \sqrt{\frac{2(\gamma_c-1)}{\gamma_c+1}}\sqrt{\left(1+\frac{\dot{m}_r}{\dot{m}_a}\right)\left(\frac{1}{\gamma_a-1}+\frac{\Delta Q_a}{\gamma_a R_a T_{ta}}+\frac{\dot{m}_r}{\dot{m}_a}\frac{\Delta Q_r}{\gamma_a R_a T_{ta}}\right)}$$
$$\left.-\left(1+\frac{1}{\gamma_a M_a^2}\right)\right] \tag{20}$$

Figure 5 shows the specific impulse and the effective specific impulse under the conditions of $(\text{O/F})_r = 8$, $C_D = 0.02$, and $S/A_a = 40$. C_D is based on a calculation result with the Newtonian model and an experimental test result [18]. S/A_a is based on the engine and airframe configurations of the present and previous studies [7]. Higher chamber pressure of the rocket results in a greater amount of rocket exhaust. With an increase of the flight Mach number, the specific impulse and the thrust coefficient decreased monotonically. The effective specific impulse of $P_c = 0.2$ MPa was larger than that of 5 MPa at low Mach numbers, whereas the impulse of 5 MPa was larger than that of 0.2 MPa in high Mach numbers.

In supersonic flight, sufficient thrust was produced with combustion of air and fuel. Higher specific impulse produced higher effective specific impulse. Large thrust assisted by the rocket was not necessary. Rather, the rocket should work as an igniter. In hypersonic flight, thrust produced only with airflow was insufficient.

C. Scramjet Mode

In hypersonic flight, the kinetic energy of air is larger than its static enthalpy. Energy conservation is approximately expressed as follows in the scramjet mode:

$$(\dot{m}_a + \dot{m}_r + \dot{m}_f)\frac{1}{2}u_c^2 \approx \dot{m}_a\frac{1}{2}u_a^2 + \dot{m}_a\Delta Q_a + \dot{m}_r\Delta Q_r \tag{21}$$

The fuel flow rate is explicit in the equation and a stoichiometric condition is presumed. From the equation, exhaust velocity of the combustion gas is deduced as follows:

$$u_c \approx \sqrt{\frac{2}{\dot{m}_a + \dot{m}_r + Ca\cdot\dot{m}_a}}\sqrt{\frac{1}{2}\dot{m}_a u_a^2 + \dot{m}_a\cdot\Delta Q_a + \dot{m}_r\cdot\Delta Q_r} \tag{22}$$

In hypersonic flight, momentum of gases is sufficiently larger than pressure force.

$$P_c \cdot A_c \ll \dot{m}_c \cdot u_c \tag{23}$$

$$P_a \cdot A_a \ll \dot{m}_a \cdot u_a \tag{24}$$

Under these assumptions, net force of the engine and specific impulse are expressed as follows:

$$F_{\text{eng}} = [(\dot{m}_a + \dot{m}_r + Ca\cdot\dot{m}_a)\cdot u_c + P_c\cdot A_c] - (\dot{m}_a\cdot u_a$$
$$+ P_a\cdot A_a) \approx (\dot{m}_a + \dot{m}_r + Ca\cdot\dot{m}_a)\cdot u_c - \dot{m}_a\cdot u_a \tag{25}$$

$$Isp = \frac{F_{\text{eng}}}{\dot{m}_r + \dot{m}_f} = \frac{\dot{m}_a + Ca\cdot\dot{m}_a + \dot{m}_r}{\dot{m}_r + Ca\cdot\dot{m}_a}\cdot u_c - \frac{\dot{m}_a}{\dot{m}_r + Ca\cdot\dot{m}_a}\cdot u_a \tag{26}$$

The choking condition of the combustion gas is not applied to the exit of the engine in the scramjet mode. The effective impulse function is expressed as follows:

$$Isp_e \approx \left(\frac{\dot{m}_a + Ca\cdot\dot{m}_a + \dot{m}_r}{\dot{m}_r + Ca\cdot\dot{m}_a}\cdot u_c - \frac{\dot{m}_a}{\dot{m}_r + Ca\cdot\dot{m}_a}\cdot u_a\right)$$
$$\times\left(1 - \frac{(1/2)C_D(S/A_a)}{[(\dot{m}_a + \dot{m}_r + Ca\cdot\dot{m}_a)/\dot{m}_a](u_c/u_a) - 1}\right) \tag{27}$$

Effective specific impulse was calculated with Eq. (27) under the conditions of $(\text{O/F})_r = 8$. In Fig. 6, flight Mach number was a parameter. As the ratio of the rocket mass flow rate increased, the specific impulse decreased and the thrust coefficient increased monotonically (not shown here). Though the effective specific impulse at lower flight Mach numbers decreased with the increase of the mass flow ratio of the rocket exhaust to airflow, the effective specific impulse increased with the mass flow ratio for Mach numbers larger than eight.

The mass flow ratio that maximizes the effective specific impulse is attained by differentiation of Eq. (27). As shown in Eq. (22), u_c is also a function of the mass flow ratio. Its differentiation is as follows:

$$\frac{du_c}{dr} = \frac{1}{\sqrt{2}}\frac{1}{(1+r+C_a)^{3/2}}\frac{1}{\sqrt{(1/2)u_a^2 + \Delta Q_a + r\cdot\Delta Q_r}}$$
$$\times\left[\Delta Q_r(1+C_a) - \frac{1}{2}u_a^2 - \Delta Q_a\right] \tag{28}$$

$$r = \frac{\dot{m}_r}{\dot{m}_a} \tag{29}$$

The differentiation of Isp_e is as follows:

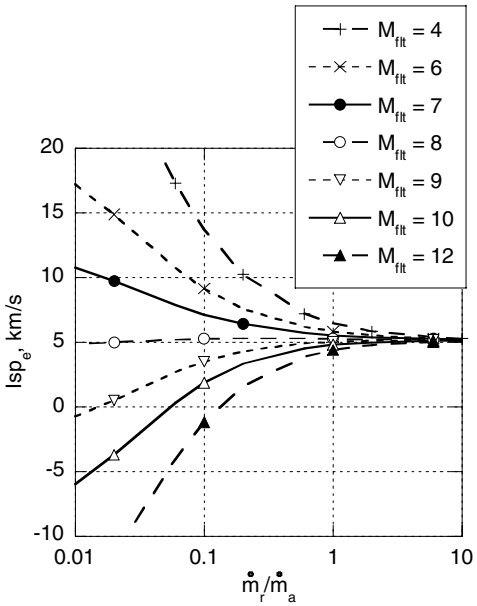

Fig. 6 $Isp \cdot (1 - F_{eng}/D)$ **term in the scramjet mode. Flight Mach number is a parameter.**

$$\frac{dIsp_e}{dr} = \frac{1}{(r+C_a)^2} \cdot \frac{1}{[(1+r+C_a)(u_c/u_a)-1]} \left\{ (u_a - u_c) \times \left[(1+r+C_a)\frac{u_c}{u_a} - 1 - \frac{1}{2} C_D \frac{S}{A} \right] + (r+C_a)\frac{1}{2} C_D \frac{S}{A} u_c + (1+r+C_a)(r+C_a) \left[(1+r+C_a)\frac{u_c}{u_a} - 1 - \frac{1}{2} C_D \frac{S}{A} \right] \frac{du_c}{dr} + (1+r+C_a)(r+C_a)\frac{1}{2} C_D \frac{S}{A} \frac{du_c}{dr} \right\} \quad (30)$$

Figure 7 shows the mass flow ratio that maximizes the effective specific impulse. The ratio existed in a narrow Mach number region around 8.3. These indicated that a smaller amount of the rocket exhaust and a higher specific impulse are preferable at low Mach numbers, whereas a larger amount of rocket exhaust and greater thrust coefficient are preferable at high Mach numbers, as well as in the ramjet mode.

IV. Simulation Methods

The preceding discussion results are examined with numerical simulation of operation of the rocket-ramjet combined-cycle engine on an SSTO plane.

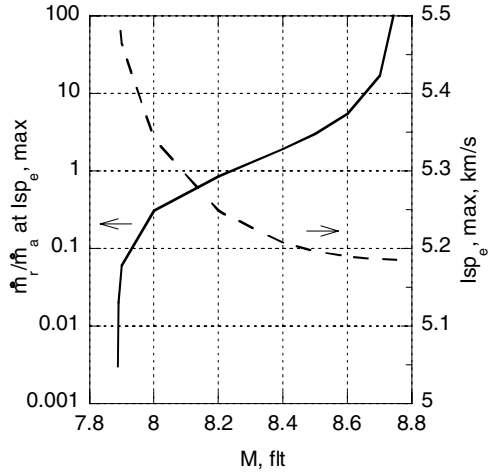

Fig. 7 Mass flow ratio that gives maximum $Isp \cdot (1 - F_{eng}/D)$ **and the maximum value.**

A. SSTO Plane

Figures 1 and 3 show the configurations and lengths of the SSTO aerospace plane and the engine used in the simulation. Mass of the plane at takeoff was 460 Mg, the same as in the previous study [7]. The length from the leading edge of the airframe to the engine was 30 m. The windward surface of the airframe forebody was 3 deg from the airframe axis. There were five engine modules on the windward surface of the plane. The height of the engine was 2 m at both the entrance and the exit. The height of the external nozzle was 7 m.

The leading edge should be sharp to decrease drag and to increase mass and momentum of the airflow to the engine. The sharp leading edge can be actively cooled [7,16,19,20]. The body of the plane was covered by a passive thermal protection system of ceramic tile.

The turbulent boundary layer on the windward surface of the airframe was calculated with an assumption of a 1/7 power velocity profile and with a friction coefficient calculated with the formula of White [21]. According to the NASP criterion on the boundary layer transition, the boundary layer was turbulent at the entrance of the engine [22]. The primary flow was assumed to be two-dimensional on a flat plate. In the subsonic airflow, the incoming air conditions were used for the conditions on the windward surface, whereas in the supersonic flow, airflow conditions after the shock wave from the airframe leading edge were used. The airflow rate into the engine was calculated based on displacement thickness of the boundary layer.

B. Combined-Cycle Engine

In the present engine, the inlet geometry was fixed during flight. The ramp wall of the inlet was assumed to be movable to thermally protect the leading edge of the cowl in the entry mode as shown in Fig. 2 [16]. The combustor geometry was fixed and there was no second throat at the exit of the engine. The operating conditions of the ejector rockets, e.g., the mixture ratio and the chamber pressure, were fixed at several levels. The hydrogen fuel flow rate from the second injector was changed to attain sufficient thrust in the ejector-jet mode and the ramjet mode.

In the inlet, two-dimensional oblique shock relations were used to calculate captured airflow rate at supersonic speed. A one-dimensional flow model was used to calculate the state properties of the airflow and combustion gas flow in the engine. Inlet performance was also calculated one-dimensionally with the kinetic energy efficiency. The expansion of the combustion gas in the external nozzle was calculated with the two-dimensional Prandtl–Meyer function. The combustion gas was in a condition of equilibrium in the engine and in a frozen condition in the external nozzle. The interaction between the airflow and the ejector rocket exhaust in the upstream combustor section was calculated with a simple model explained later. The friction coefficient of the turbulent boundary layer on the engine was calculated by the formula of White [21].

Low flight-dynamic pressure of the SSTO plane is preferable from structure strength and thermal protection, whereas high pressure is preferable from engine thrust production and payload to an orbit [19]. In the present study, as in the previous studies [7], 50 kPa was adopted. The engine geometry and the operating conditions were designed for flight with this dynamic pressure of 50 kPa. A low contraction ratio of inlet is favorable for supersonic speed operation around Mach 3 to capture air, whereas a high ratio is favorable for hypersonic operation higher than Mach 5. The contraction ratio becomes smaller downstream of the rocket nozzles. Herein, the contraction ratio of the inlet was set to be 4.6. As mentioned in the preceding section, in the subsonic speed, the augmentation of thrust by airbreathing was not sufficient. Therefore, the engine operated in the rocket mode at takeoff and during subsequent subsonic flight. The mode changed to the ejector-jet in the transonic condition.

1. *Ejector Rocket*

Each engine module had four ejector rockets, and thus there were a total of 20 rockets on the vehicle. The mixture ratio O/F was 7.0 in the ejector-jet, ramjet, and rocket modes. The mixture ratio O/F of 7 was adopted to attain a sufficient efficiency of the secondary combustion. In the scramjet mode, the mixture ratio was set so that

the equivalence ratio of the residual hydrogen in the rocket exhaust to air became almost unity.

Reference chamber pressure was set to be 7 MPa and the throat diameter of each rocket was 0.14 m. The pressure and the diameter were specified to produce sufficient thrust to breath air in the transonic condition and to accelerate the SSTO plane in the rocket mode.

2. Inlet

The inlet had a ramp-compression system. The ramp angle was 8 deg. This configuration was specified so as not to induce separation of the boundary layer. The captured mass flow rate was calculated with the ramp shocks in the supersonic flow condition. A bent cowl was adopted to enlarge the starting condition of the inlet to a lower Mach number [8]. The cowl leading edge was located 1 m upstream of the entrance of the throat section. The total pressure was maintained in the subsonic condition in the inlet, whereas the kinetic energy efficiency was 0.98 in the supersonic flow condition. In the unstarted condition, a normal shock was located on the ramp ahead of the cowl when the oblique shock wave was attached to the ramp corner of the inlet. When the shock was not attached to the corner, a normal shock was located ahead of the inlet. Subsonic air flowed into the engine.

In the rocket mode, the engine performance was calculated under the inlet-open condition. It was planned that the inlet would be closed during the ascent flight or in an orbit in a low flight-dynamic pressure condition.

3. Upstream Combustor

In the ejector-jet mode, the momentum exchange between the breathed air and the rocket exhaust in the upstream combustor section downstream of the rocket nozzle was calculated with a simple model [7,17]. In the model, momentum was transferred from air to rocket exhaust or from rocket exhaust to air through the dividing streamline. After the interaction, the air and the rocket exhaust flowed in parallel one-dimensionally at the same pressure with conservation of mass, impulse function, and energy. When inflow air was in subsonic speed, a flow rate of the breathed air was determined through this interaction.

In the scramjet mode, the rocket exhaust reacted with the air in this section. In this study, several kinds of operating conditions of the rocket were specified so that an equivalence ratio of the residual hydrogen to air became almost unity.

In the rocket mode, if there was airflow into the engine, the rocket exhaust further reacted with the air in the same manner as in the scramjet mode. In a vacuum, combustion gas did not flow into the inlet, and the pressure in the inlet and the throat section was zero. The rocket exhaust expanded at the exit of the rocket nozzle with no reaction force from the throat section, and then the gas expanded in the divergent section isentropically.

4. Second Fuel Injector and Choking Condition

In the ejector-jet and ramjet modes, subsonic combustion was attained with fuel from the second injector, and the choking condition was assigned at the exit of the engine. The mass of the combustion gas was the sum of those of the rocket exhaust, fuel, and air. Total energy was also the sum of those of the rocket exhaust, fuel, and air. Impulse function was specified at the exit of the engine with the mass, energy, and the choking condition. The downstream combustor section was a straight duct and had the same cross section as that at the entrance of the engine. The rocket exhaust and the air were presumed to be mixed by the end of the divergent section. The condition of the mixture in the straight duct before the secondary combustion was calculated under conservations of mass, momentum, and energy which were the same as those at the exit of the engine, except mass and energy of the secondary fuel.

In the scramjet mode and the rocket mode, there was no fuel injection from the second injector. Choking was not assigned at the exit of the engine.

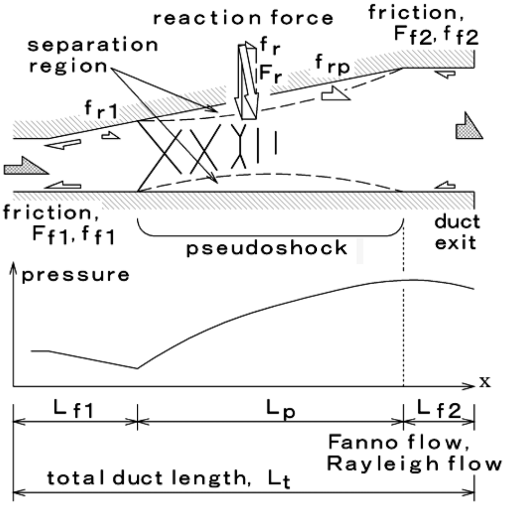

Fig. 8 Schematic of flow with pseudoshock.

5. Divergent Section

In the ejector-jet mode and the ramjet mode, the airflow and the rocket exhaust individually expanded isentropically until the starting position of the pseudoshock in the divergent section. Based on balance of the impulse function, the starting position of the pseudoshock was calculated [13]. A schematic of the flow with the pseudoshock is shown in Fig. 8. The starting position of the pseudoshock was located so that the sum of the inflow impulse functions of the air and the rocket exhaust and the reaction force from the engine wall was equal to the function of the mixture before the secondary combustion, which was specified by the choking condition at the engine exit. In the momentum balance model, friction force was presumed to be none in the pseudoshock. The pressure was presumed to be linearly distributed in the pseudoshock because specification of pressure was conducted only at the points of beginning and end of the pseudoshock in this model.

In the scramjet mode and the rocket mode, the combustion gas flowed isentropically in the divergent section.

C. Simulation of Flight Conditions

The flight conditions with the combined-cycle engine were investigated with a simulation of SSTO aerospace plane flight to a low Earth orbit of 100 km. The simulation methods of the flight of the plane were the same as those used in a previous investigation [23]. The aerospace plane was treated as a material point. The flight path was on a two-dimensional plane. The aerodynamic data of the plane were from [18]. The flight-dynamic pressure was 50 kPa in the reference condition during the airbreathing propulsion mode.

V. Simulation Results and Discussion

Figures 9 and 10 show specific impulses and thrusts of the engine used in the simulation. The thrust is plotted as a form of the thrust coefficient with the flight-dynamic pressure and the projected cross section of the engine at the entrance. In the ramjet mode, the choking condition of the combustion gas at the engine exit was searched by a discrete increase of fuel from the second injector, so the impulse and coefficient of the ramjet mode did not change smoothly. Three operating conditions in the ramjet mode and four in the scramjet mode of the rocket were examined. Their chamber pressures and mixture ratios are listed in Table 1. In the ramjet mode, ram–1 had the highest specific impulse and the lowest thrust coefficient, whereas ram–3 had the lowest specific impulse and the highest thrust coefficient. In the scramjet mode, scram–1 had the highest specific impulse and the lowest thrust coefficient, whereas scram–4 had the lowest specific impulse and the highest thrust coefficient.

Thrust coefficient of the ejector-jet mode became great due to small dynamic pressure in low-speed condition, whereas specific impulse slightly increased in subsonic speed from 3000 $\mathrm{m \cdot s^{-1}}$ at

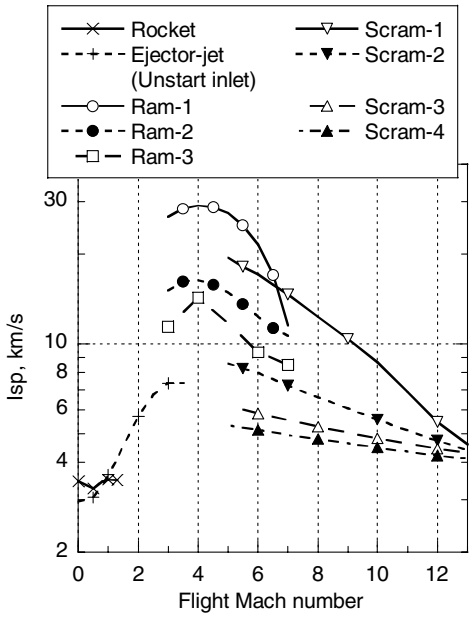

Fig. 9 Specific impulses of the combined-cycle engine.

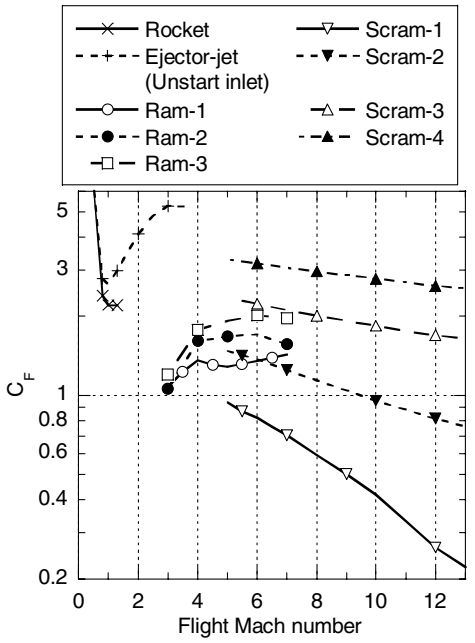

Fig. 10 Thrust coefficients of the combined-cycle engine.

takeoff to 3600 $m \cdot s^{-1}$ at the flight Mach number of one. That is, the thrust augmentation effect of the engine did not change greatly within this subsonic speed, as the analytical investigation made clear as shown in Fig. 4.

Flight simulation was conducted with these engine performances. The operating mode was changed to attain a larger amount of mass carried into orbit. Figures 11 and 12 show masses and velocities of the SSTO aerospace plane for engine operating conditions. The rocket mode was used from takeoff to about Mach 0.6 and after the

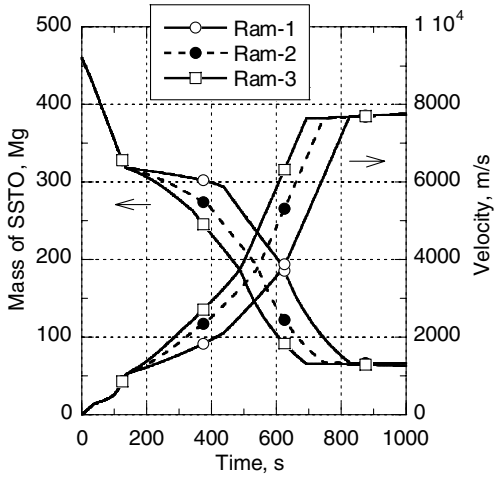

Fig. 11 SSTO plane mass and velocity. The scramjet mode used scram–3 performances.

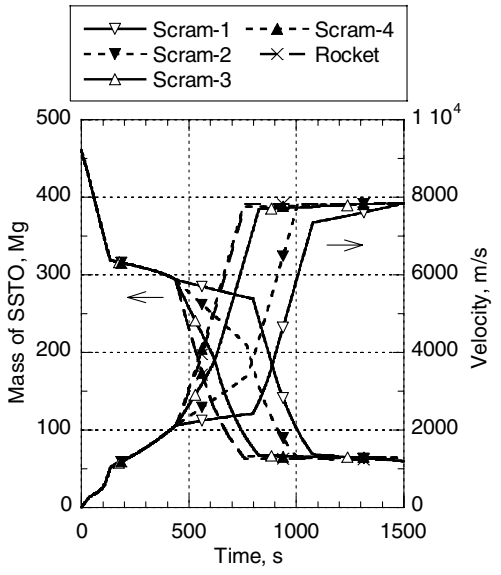

Fig. 12 SSTO plane mass and velocity. The ramjet mode used ram–1 performances.

scramjet mode in every flight. In the simulation of the rocket in Figs. 11 and 12, the rocket engine with O/F = 7 and $P_c = 7$ MPa operated with secondary combustion of residual fuel in the rocket exhaust with air from Mach 7 to 11.

Figure 13 shows a comparison of the mass carried into the orbit. Scram–3 was used in the examination of the ramjet modes, whereas ram–1 was used in the examination of the scramjet modes. In the ramjet mode, change from the ramjet mode to the scramjet mode was conducted at Mach 7 in ram–1, whereas this was done at Mach 8 in ram–2 and ram–3. The average density of propellants during the whole flight was, for example, 370 $kg \cdot m^{-3}$ in the flight with ram–1 and scram–3. Ram–1, with the highest specific impulse, showed transportation of the largest mass into orbit, though the flight time was longest as shown in Fig. 11. Ram–2 and ram–3 had larger thrust coefficient than ram–1, so the operating Mach number range became

Table 1 Operating conditions of rocket in each engine

	Ram–1	Ram–2	Ram–3	Scram–1	Scram–2	Scram–3	Scram–4	Rocket
P_c, MPa	0.2	0.6	1.0	0.4	2.0	4.5	7.0	7.0
O/F	7.0	7.0	7.0	0.5	2.5	4.5	5.5	7.0

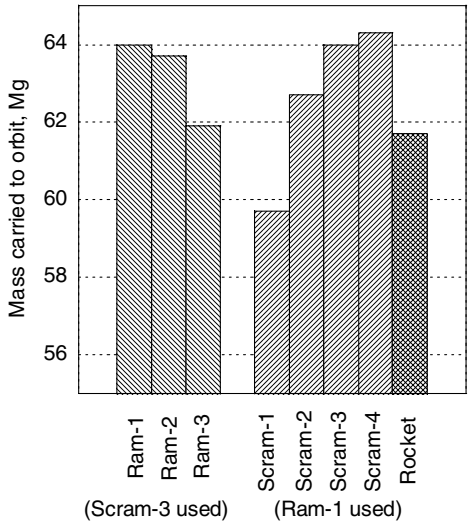

Fig. 13 Mass transported to orbit. For rocket, P_c and O/F were 7 MPa and 7, respectively.

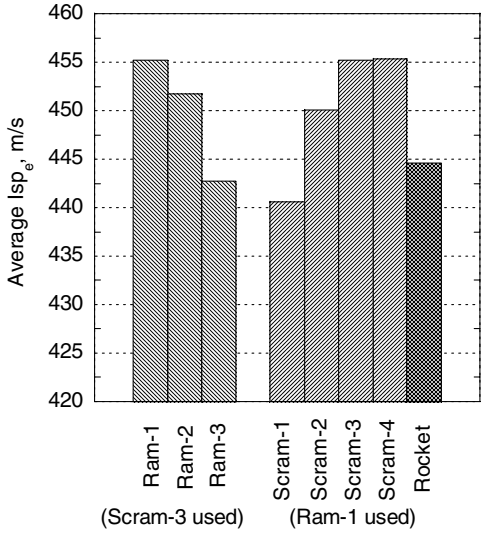

Fig. 14 Average effective specific impulse.

larger. However, even with larger range, the engine with a lower specific impulse could not carry a larger mass into orbit.

In the scramjet mode, scram–4 with the highest thrust carried the largest amount of mass into orbit. In scram–1, change from the scramjet mode to the rocket mode occurred at Mach 8. In scram–2, it took place at Mach 11. In scram–3 and scram–4, it happened at Mach 12. In case of rocket, the equivalence ratio was about 0.8, and the effect of combustion of residual fuel in the rocket exhaust on thrust augmentation was smaller than that in scram–4, even with the same chamber pressure.

Figure 14 shows comparison of the average value of the effective specific impulse. Its definition is as follows:

$$Isp_{e,\mathrm{av}} = \frac{\int (F - D)\,\mathrm{d}t}{\int \dot{m}_p\,\mathrm{d}t} \tag{31}$$

The combination of ram-1 and scram-4 showed the greatest value. Higher specific impulse in the ramjet mode and larger thrust in the scramjet mode caused a greater effective specific impulse, resulting in a larger amount of mass being carried into orbit, as pointed out in the analytical study.

In the present study, analytical investigation used highly idealized assumptions, and the simulation of the engine operation used physical models and several assumptions. Though the calculated engine performances had insufficient accuracy, the criterion on the engine operation in supersonic and hypersonic flights had sufficient validity. Kauffman et al. [24] conducted simulation of an SSTO plane with an airbreathing engine and a rocket engine . They showed that airbreathing propulsion was more effective than rocket propulsion in the supersonic speed range and concurrent airbreathing/rocket propulsion was effective to reduce fuel/propellant consumption in the hypersonic speed range. Yokoyama et al. [25] also showed necessity of concurrent use of a dual-mode engine and a rocket engine in the hypersonic range. These support the criterion on the engine operation of this study; higher specific impulse was preferable in supersonic flight, whereas greater thrust was preferable in hypersonic flight.

VI. Conclusions

Operating conditions of a rocket-ramjet combined-cycle engine for a single-stage-to-orbit aerospace plane were studied. The engine was composed of an ejector-jet mode, a ramjet mode, a scramjet mode, and a rocket mode. First, characteristics of each operating mode were examined analytically. Then, flight simulation was conducted with various engine performances. From these studies, the following points were clarified:

1) From the analytical study, the thrust augmentation effect of the ejector-jet mode was found to be small at low subsonic speed. The effect increased with an increase of the flight Mach number, especially in the supersonic condition.

2) From another analytical study, higher specific impulse was shown to be preferable in supersonic flight, whereas greater thrust coefficient was preferable in hypersonic flight to attain a greater velocity increment.

3) Simulation of engine operation and flight of an SSTO plane proved the analytical results. That is, higher specific impulse in the ramjet mode and greater thrust in the scramjet mode resulted in a greater effective specific impulse and a larger amount of mass being carried into orbit.

References

[1] Bertin, J. J., *Hypersonic Aerothermodynamics*, AIAA Education Series, AIAA, Washington, DC, 1994, pp. 592–594.

[2] Escher, W. J. D., "User's Primer for Comparative Assessments of All-Rocket and Rocket-Based Combined-Cycle Propulsion Systems for Advanced Earth-to-Orbit Space Transport Applications," AIAA Paper 95-2474, July 1995.

[3] Olds, J. R., and Bradford, J. E., "SCCREAM: A Conceptual Rocket-Based Combined-Cycle Engine Performance Analysis Tool," *Journal of Propulsion and Power*, Vol. 17, No. 2, 2001, pp. 333–339.

[4] Heiser, W. H., Pratt, D. T., Daley, D. H., and Mehta, U. B., *Hypersonic Airbreathing Propulsion*, AIAA Education Series, AIAA, Washington, DC, 1994, pp. 447–451.

[5] Faulkner, R. F., "Integrated System Test of an Airbreathing Rocket (ISTAR)," AIAA Paper 2001-1812, April 2001.

[6] Siebenhaar, A., "Strutjet Evolves to Meet Air-Breathing Propulsion Challenges for the 21st Century," *13th International Symposium on Air-Breathing Engines*, Paper 97-7135, Sept. 1997.

[7] Kanda, T., and Kudo, K., "Conceptual Study of a Combined-Cycle Engine for an Aerospace Plane," *Journal of Propulsion and Power*, Vol. 19, No. 5, 2003, pp. 859–867.

[8] Kubota, S., Masuya, G., and Tani, K., "Aerodynamic Performances of the Combined Cycle Inlet," *24th International Congress of Aeronautical Sciences*, International Council of the Aeronautical Sciences Paper 2004-6.6.1, Yokohama, Japan, Sept. 2004.

[9] Tani, K., Kanda, T., and Tokudome, S., "Aerodynamic Characteristics of the Combined Cycle Engine in an Ejector Jet Mode," AIAA Paper 2005-1210, Jan. 2005.

[10] Kanda, T., Kato, K., Tani, K., Kudo, K., and Murakami, A., "Experimental Study of a Combined-Cycle Engine Combustor in Ejector-Jet Mode," AIAA Paper 2006-0223, Jan. 2006.

[11] Kato, K., Kanda, T., Kobayashi, K., Kudo, K., and Murakami, A., "Downstream Ramjet-Mode Combustion in a Dual-Mode Scramjet Engine," *Journal of Propulsion and Power* (to be published).

[12] Kato, T., Kanda, K., Kato, K., and Murakami, A., "Experimental Study of Combined Cycle Engine Combustor in Scramjet Mode," AIAA Paper 2005-3316, May 2005.

[13] Kanda, T., and Tani, K., "Momentum Balance Model of Flow Field with Pseudo-Shock," AIAA Paper 2005-1045, Jan. 2005.
[14] Chinzei, N., Masuya, G., Kudo, K., Murakami, A., and Komuro, T., "Experiment on Multiple Fuel Supplies to Air Breathing Rocket Combustors," *Journal of Propulsion and Power*, Vol. 3, No. 1, 1987, pp. 26–32.
[15] Masuya, G., Chinzei, N., and Ishii, S., "Study of Air Breathing Rockets: Subsonic Mode Combustion," *Acta Astronautica*, Vol. 8, Nos. 5–6, 1981, pp. 643–661.
[16] Kanda, T., and Kudo, K., "Cooling Requirement of Combined Cycle Engine in Descending Flight," *Proceedings of 24th International Symposium on Space Technology and Science*, Japan Society for Aeronautical and Space Sciences, Tokyo, 2004, pp. 39–44.
[17] Aoki, S., Lee, J., Masuya, G., Kanda, T., and Kudo, K., "Aerodynamic Experiment on an Ejector-Jet," *Journal of Propulsion and Power* (to be published).
[18] Nomura, S., Hozumi, K., and Kawamoto, I., "Experimental Studies on Aerodynamic Characteristics of SSTO Vehicle at Subsonic to Hypersonic Speeds," *Proceedings of the 16th International Symposium on Space Technology and Science*, Committee of International Symposium on Space Technology and Science, Tokyo, 1988, pp. 1547–1554.
[19] Kanda, T., and Kudo, K., "Preliminary Study of Thermal Protection System of a Single-Stage-to-Orbit Plane," *Proceedings of the 22nd International Symposium on Space Technology and Science*, Japan Society for Aeronautical and Space Sciences, Tokyo, 2000, pp. 1354–1360.
[20] Kudo, K., and Kanda, T., "Preliminary Study of Thermal Protection System of a Single-Stgae-to-Orbit Plane (2)," *Proceedings of the 23rd International Symposium on Space Technology and Science*, Japan Society for Aeronautical and Space Sciences, Tokyo, 2002, pp. 1075–1080.
[21] White, F. M., *Viscous Fluid Flow*, McGraw–Hill, New York, 1974, pp. 642–644.
[22] Berry, S. A., Auslender, A. H., Dilley, A. D., and Calleja, J. F., "Hypersonic Boundary-Layer Trip Development for Hyper-X," *Journal of Spacecraft and Rockets*, Vol. 38, No. 6, 2001, pp. 853–864.
[23] Kanda, T., and Kudo, K., "Payload to Low Earth Orbit by Aerospace Plane with Scramjet Engine," *Journal of Propulsion and Power*, Vol. 13, No. 1, 1997, pp. 164–166.
[24] Kauffman, H. G., Grandhi, R. V., Hankey, W. L., and Belcher, P. J., "Improved Airbreathing Launch Vehicle Performance with the Use of Rocket Propulsion," *Journal of Spacecraft and Rockets*, Vol. 28, No. 2, 1991, pp. 172–178.
[25] Yokoyama, N., Suzuki, S., Tsuchiya, T., Taguchi, H., and Kanda, T., "Multidisciplinary Design Optimization of SSTO Space Plane Considering Rigid Body Characteristics," AIAA Paper 2005-0710, Jan. 2005.

L. Maurice
Associate Editor